Influence and Evaluation of Potential Fractured Zone by Surrounding Rockmass Deformation during Deep Tunneling Blasting Excavation

Jixue Zhou[1,2], Junhong Huang[1,3,4], Yi luo[1] and Xinping Li[1]

[1]*Hubei Key Laboratory of Roadway Bridge and Structure, Wuhan University of Technology, Wuhan, China*
[2]*School of Civil Engineering and Architecture, Wuhan University of Technology, Wuhan, China*
[3]*School of Safety Science and Emergency Management, Wuhan University of Technology, Wuhan, China*
[4]*School of Resource, Environmental Science and Engineering, Hubei University of Science and Technology, Xianning, China*

Keywords: Deep Tunnel, Rockmass Excavation, Longitudinal Deformation Curve, Fractured Band, Settlement Monitoring.

Abstract: Daliang tunnel on Lanzhou-Xinjiang high-speed railway is a typical tunneling project with adverse geological conditions, especially fractured zones during blasting excavation. A major collapse disaster was caused due to an unexpected fractured zone, which was excavated and supported improperly. Field test data of surrounding rockmass displacement is analyzed for changes alone tunnel axis and with time. Deformation curve versus time for tunnel sections with surrounding rockmass in consistent and relatively high integrity shows one inflection point, where deformation rate changes from increase to decrease. It revealed by numerical analysis that before exposed by blasting excavation, rockmass near fractured zone has shown much deformation. Inflection point can always by observed on the total deformation curve, while it appears earlier when nearer to the fractured zone. When the inclination angle of the fractured zone is small, the location of inflection point on deformation-time curve is more sensitive to the change of inclination angle. Existence of a fractured zone in vicinity ahead can be evaluated for choosing proper blasting excavation and support method.

1   INTRODUCTION

With the continuous development of the Belt and Road initiative, construction of Chinese transportation projects have been further developed. High-speed railway network are extending in West China along the Silk Road and through Qinghai-Tibet Plateau and Xinjiang, where geological conditions are complex. Deformation and stability of deep-buried tunnels in complicated geological conditions are often controlled by fault fractured zone (Lenz et al, 2017), such as similar cases in the world-famous Tauern Tunnel and the Arlberg Tunnel (Austria), and the Enasan Tunnel (Japan), during excavation. Fault fractured zone problems are also often encounter during tunnel blasting excavation in recent years. Kun and Onargan (2013) studied the influence of fractured zone for Izmir Metro Tunnel, and determined risky area in the tunnel. A Case Study on Nowsoud Tunnel fractured zones would determine the stress distribution in adjacent tunnel section, and predicted squeezing potential for a critical zone (Fatemi et al, 2016). Zhao et al (2013) studied highly risky tunnels in Guiyang-Guangzhou high-speed railway, and developed a method for detecting fractured zone in karst area. Zhang et al (2014) have focused on issues in excavating the deep and long Taining tunnel, South China, where several squeezing fault zones have to be tunneled through, and large deformations were frequently encountered during excavation. It is demonstrated by previous studies that, fractured zones have great influence on surrounding rockmass integrity in vicinity, thus surrounding rockmass deformation characteristic is different.

Lisjak et al (2015) argued that the characteristics of rockmass have great influence on the characteristic of near field deformation base on the analysis of the monitoring data about deformation from Mont Terri underground research laboratory. Moffat et al (2015) studied the axial strain of roadway and distribution law based on fiber grating equipment. Lin et al (2017)

investigated the characteristics of strike-slip faults and displacement in Yanmenguan Tunnel, and revealed that quality of surrounding rock masses should be carefully identified, since it can be greatly influenced by faults nearby and is critical to rockmass deformation.

In the aspect of calculating the deformation distribution of longitudinal profile, many scholars have studied the deformation release coefficient method and the support force coefficient method (Cai et al, 2015; Lu et al, 2014). Alejano et al (2012) calculated the numerical calculation of the rockmass within a certain GSI (geological strength index) based on the ideal elasto-plastic assumption, and proposed a simplified formula for calculating the radius of the plastic zone of the surrounding rockmass to optimize the Calculation method of deformation distribution of strain softening longitudinal section. Vlachopoulos and Diederichs (2009) optimized the deformation energy analysis calculation about the longitudinal profile of surrounding rock, which is based on the further study of the final radial plastic deformation calculation method.

In the numerical analysis, Zhao et al (2015) analyzed the variation of surrounding rockmass deformation along with the tunnel axis during soft rock tunneling based on numerical calculation. Basarir et al (2010) considers the influence of rock mass characteristics, tunnel size and force state of surrounding rockmass of the face tunnels, and uses the Three-Dimensional Finite Element Analysis to calculate the deformation distribution of the longitudinal profile of the tunnel and put forward the fitted formula.

This paper is aiming at the fault fractured zone with smaller thickness and strike perpendicular to the axis of the tunnel, so as to explore the deformation evolution characteristics of surrounding rockmass caused by tunnel blasting excavation near a fault, by analyzing field test data and numerical calculation of surrounding rock deformation.

2 DEFORMATION CHARACTERISTICS OF DALIANG TUNNEL BLASTING EXCAVATION

Lanzhou-Xinjiang high-speed railway (from Lanzhou to Urumqi), also known as The "Iron Silk Road", is the longest railway ever built in the world with full length for 1776 km. Along this railway, Daliang tunnel starts from DK328+820 and ends at DK335+370, with length for 6550m. It's a double-line tunnel with large section, the excavation height is 13m and the excavation span is 15m. The track gradient inside the tunnel lies between 6 ‰－9 ‰. Apart from the entrance point located on the curve, the rest are located on straight line. Tunnel goes through the Qilian Mountain (elevation more than 4000m) ,with the maximum buried depth for more than 600m.

At the time of assisting main tunnel construction, the tunnel section in 465m depth has faced serious large abrupt deformation due to blasting excavation. The maximum deformation rate reached 41mm/d, which led to cracking of initial support and dropping of concrete. Deformation of surrounding rockmass is not convergent. Design reports show that surrounding rockmass of this section should be Class IV, but in fact it is crashed thin layer black slate with developed joints. Surrounding rockmass has obvious tectonic extrusion characteristic, and is in poor stability (Figure 1). Large deformation was observed in surrounding rockmass after application of original construction design.
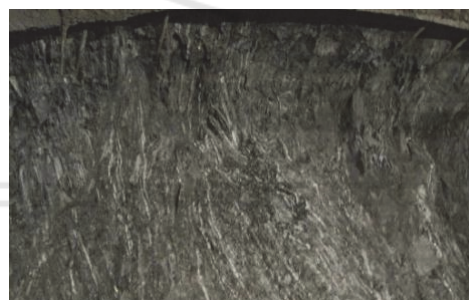

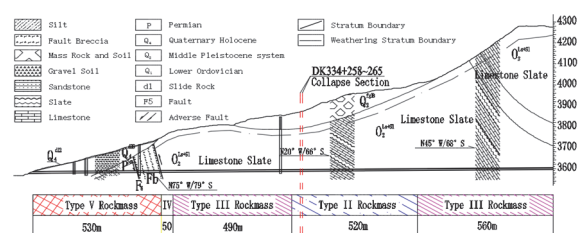Figure 1: The actual surrounding rockmass exposed by excavation.

Figure 2: Longitudinal section of exit section of Daliang tunnel.

Maximum daily settlement of DK331+885 section is 56mm, maximum daily convergence value is 30.8mm. Maximum settlement and convergence of DK331+766 section values are up to 197.5mm and 151.3mm for 4 days, with maximum daily settlement and convergence value of 45.8mm and 29.9mm.

Table 1: Classification and design excavation method for surrounding rockmass of Daliang tunnel (2010).

Tunnel Section	Rock Class	Geological Feature	Excavation and Support Method
DK332+040 ~DK332+750	III	Deep buried limestone slate in good integrity	Bench blasting, Grade III support
DK332+750 ~DK333+250	III	Deep buried limestone slate in good integrity	Short bench blasting. Enhanced Grade III lining
DK333+250 ~DK333+780	III	Deep buried limestone slate in good integrity	Bench blasting, Grade III support
DK333+780 ~DK334+300	II	Deep buried limestone slate in good integrity	Full-face blasting, Grade II support
DK334+300 ~DK334+590	III	Deep buried limestone slate in good integrity	Bench blasting, Grade III support
DK334+590 ~DK334+790	III	Deep buried limestone slate in good integrity	Short bench blasting. Grade III lining.
DK334 +790 ~DK334+840	IV	Influenced by Fault F5. Limestone slate rich of fractures	Three-bench blasting in seven steps. Grade IV lining.
DK334+840 ~DK335+370	V	Fractured zone at Fault F5. Fault breccia	CRD blasting method. Grade V lining.

As described in the Tunnel Risk Assessment Report (Figure 2 and Table 1), the exit of Daliang Tunnel at DK334+300 ~ DK333+780 was initially designed for Middle Ordovician limestone sandwich plate and Class II surrounding rockmass in good integrity, using full-face method and Class II rockmass lining. However, during the excavation process, obvious loosening and broken rockmass is found after blasting excavation. Even after adopting bench method and Class III lining conservatively, it still generated large deformation in surrounding rockmass after excavation.

When blasting excavating to DK334+241 section, collapse of surrounding rockmass took place in 17~24m distance to excavation face. The primary supporting frame squeezed off, with about 185m³

rockmass fragments swarmed into the tunnel (Figure 3), forming a cavity 3.5m in depth, 6m in height and 7m in length. The collapse section showed obvious crushed carbonaceous slate layers formed by strong tectonic movement, which constantly collapsed in an unstable state. Within 10m distance to the collapse area, shot concrete layer cracked in several locations, including severe dropping off at the dome. The maximum convergence value for side wall was 1m, and primary support had intruded the limit. Monitoring measurement on the sidewall shows that collapse in surrounding rockmass had led to large deformation. Settlement and the convergence value raise up to 36.4mm and 57.6mm on the same day, 5m distance to the collapse.
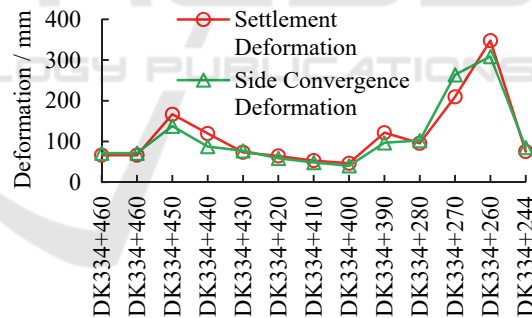

Figure 3: Collapse due to a fractured zone.

Figure 4: The surrounding rockmass deformation in vicinity of the fractured zone.

From long-term observation of accumulative settlement and convergence deformation values around the surrounding rockmass in this section (Figure 4), the accumulated deformation in surrounding rock mass of this section is much larger than that of other tunnel sections. Obviously, accurate judgment on the type of rockmass and identifying potential fractured zone ahead is significant in choosing proper blasting excavation methods, applying advanced support and controlling surrounding rockmass deformation and stability.

3 DEFORMATION DISTRIBUTION CHARACTERISTICS OF TUNNEL EXCAVATION

3.1 Abrupt Deformation Mechanism Induced by Integrity Change of Tunnel Surrounding Rockmass

Previous studies on deformation distribution caused by tunnel blasting excavation have more concern to tunnel cross section. According to the Kastner Equation 1 (Cui et al, 2014), plastic zone boundary deformation u* and tunnel wall deformation u can be calculated in Equation 2 and 3, if the shear expansion of surrounding rocks is ignore.

$$\frac{R_p}{R_0} = \left[\frac{\sigma_0(1-\sin\varphi)-c\cdot\cos\varphi+c\cdot ctg\varphi}{p_i+cctg\varphi}\right]\exp(\frac{1-\sin\varphi}{2\sin\varphi}) \quad (1)$$

$$u^* = \frac{1+\mu}{E}R_p(\sigma_0\sin\varphi+c\cdot\cos\varphi) \quad (2)$$

$$u = \frac{R_p}{R_0}u^* + \frac{K(R_p^2-R_0^2)}{2R_0} \quad (3)$$

where, R_0 is tunnel radius, R_p is plastic zone radius, σ_0 is initial in-situ stress, P_i is support resistance, φ is internal friction angle, μ is Poisson's ratio, E is elastic modulus, and K is plastic zone shear coefficient.

It can be seen that tunnel wall deformation is approximately proportional to the square of the radius of the plastic zone, and the deformation of the surrounding rock is larger when angle of internal friction is small or in-situ stress is larger. During tunnel excavation, the sudden encountering of a fractured zone is actually a sudden change in rockmass integrity in the longitudinal profile, thus will induce a large and rapid increase in deformation.

3.2 Abrupt Deformation Mechanism Induced by Integrity Change of Tunnel Surrounding Rockmass

Studies on longitudinal deformation curve (LDC) were mainly limited by the three-dimensional characteristics of this subject. Studies on convergence deformation induced by tunnel excavation were mainly about radial deformation (Carranza-Torres and Fairhurst, 2000). Under the assumption of linear elastic assumption, the radial deformation of

surrounding rockmass of circular tunnel can be expressed in polar coordinate equation:

$$U_r = \eta\frac{\sigma_1R^2(1+\mu)}{2Er}\left\{1+\lambda+(1-\lambda)\left[4(1-\mu)-\frac{R^2}{r}\right]cos(2\theta)\right\} \quad (4)$$

where, λ is the lateral pressure coefficient, μ is poisson's ratio, σ_1 is the maximum overburden pressure, η is the constraint loss.

Panet (1995) put forward:

$$\frac{U_r}{U_{max}} = \alpha_0 + (1-\alpha_0)\left[1-\left(\frac{m}{m+Z/R}\right)^2\right] \quad (5)$$

Hoek (1988) proposed:

$$\frac{U_r}{U_{max}} = \left[1+\exp\left(\frac{-Z}{1.1R}\right)\right]^{-1.7} \quad (6)$$

Most empirical formulas for longitudinal deformation variation were established based on a large amount of monitored deformation data. They can describe variation of radial deformation along unsupported tunnels. However, after considering the influence of a fractured zone in front of tunnel face, the deformation distribution on longitudinal profile is more complicated, thus numerical calculation method is adopted to carry out a three-dimensional analysis (Basarir, 2010).

4 ANALYSIS OF DEFORMATION CHARACTERISTICS OF SURROUNDING ROCKMASS NEAR FRACTURED BAND

4.1 Physical and Mechanical Parameters of Rockmass and In-situ Stress Field

Laboratory tests of the sample of rock mass were carried out. Results showed that the rockmass of fractured band was mostly formed under tectonic movement, of which the unit weight was 18.2~19.6 KN/m³. Rockmass in the fractured band has a relatively uniform gradation. Its coarse particle size filled with fine particles, thus has a higher internal friction angle and cohesion force. So, in original stable state, it can be regarded as equivalent elastoplastic body, thus the Drucker-Prager yield criterion is used to calculate the physical and mechanical parameters of the rockmass as Table 2.

Table 2: Classification and design excavation method for surrounding rockmass of Daliang tunnel.

Parameter	Fractured zone	Slate
Elastic Modulus / GPa	2.2	6.8
Poisson's Ratio	0.4	0.31
Cohesion / MPa	0.3	0.64
Internal Friction Angle / °	27	47
Unit Weight / KN/m^3	18.9	26.2

Based on the field test, the effective in-situ stress test data were obtained in the borehole at depth of 15.0m, 18.5m, 19.0m and 27.0m in the inclined shaft, as shown in Table 3. It is shown that the maximum value of maximum horizontal principal stress at the measured depth is 25.14MPa, and is approximately perpendicular to the borehole axis. The maximum value of the minimum horizontal principal stress is 13.77MPa. The maximum vertical stress is 12.30MPa. The lateral pressure coefficient is between 1.89 and 2.08, and is consistent to strata curvature observed on tunnel face. The in-situ stress is applied to the calculation model based on test results.

Table 3: Vertical drilling water pressure fracturing results (2012).

Parameter	Test section depth / m			
	15	18.5	22	27
Maximum Horizontal Principal Stress / MPa	23.55	25.14	23.04	24.81
Minimum Horizontal Principal Stress / MPa	12.95	13.45	13.77	13.37
Vertical Principal Stress / MPa	12	12.09	12.18	12.3
Lateral Pressure Coefficient	1.96	2.08	1.89	2.02

4.2 The Finite Element Analysis and Comparison of the Deformation Due to Influence of Fractured Zone

A three-dimensional finite element calculation model is established for practical engineering. The length of the model is 100m and the width is 200m. The model is meshed into 117,872 eight-node elements and 120,098 nodes. The fractured zone is meshed by smaller elements as shown in Figure 5. Element live-and-kill method is adopted in simulating excavation process, with excavation footage of 1m. Deformation evolution of surrounding rockmass at each measuring points are calculated for the process of tunneling into the fractured zone.
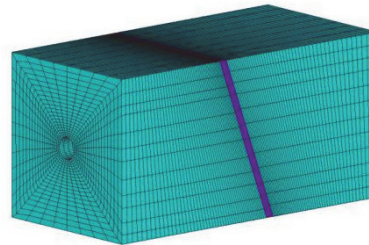

Figure 5: Finite element model.

Blasting excavation to the vicinity of the tunnel collapse section is analyzed. Judging by collapse area width and strata dip angle, the thickness of the fractured band is about 7m, and the inclination is about 66° inclination. The strike of the fractured zone is perpendicular to the excavation direction, and dip is in the same direction as excavation direction. Based on the actual excavation process, the excavation rate is 1m/d, the deformation and evolution of the surrounding rockmass of each measuring point are calculated in the process of heading into the fractured zone and compared with the measured data, as shown in Figure 6.
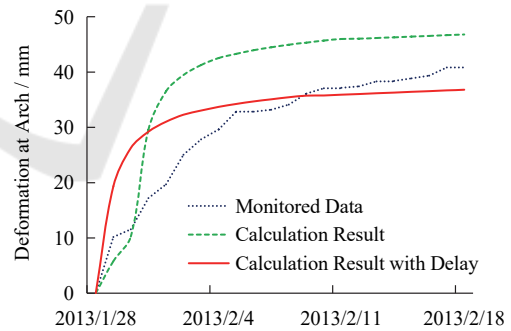

Figure 6: The calculative results compared with the measured data.

Comparison between calculated results and the measured data of the settlement of the top arch of the distance crushing zone 38m shows small difference. On the one hand, in the calculated deformation curve, obvious deformation rate increases can be observed about 1 days after the excavation of the measuring section, showing obvious inflection point on the deformation-time curve. However, no inflection point can be observed on the monitored curve. On the other

hand, the accumulative deformation value of the two curves show up to 10 mm difference on the 31st day. However, in actual excavation, when the measuring section has just been exposed, installation of monitoring points could be very risky near tunnel face. Therefore, the actual monitoring process usually starts several days after the section was exposed. Considering the above fact, the calculated excavation curve is shifted leftwards. The new curve shows consistence with the monitored curve in deformation trend and value.
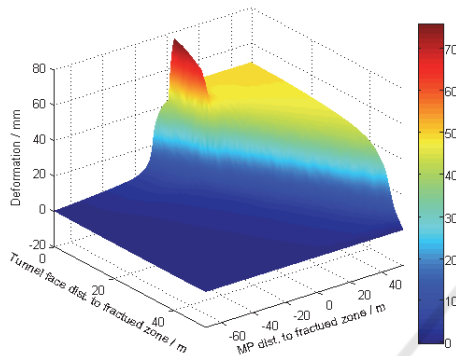

Figure 7: The accumulative settlement of the measured points as tunneling proceeding.
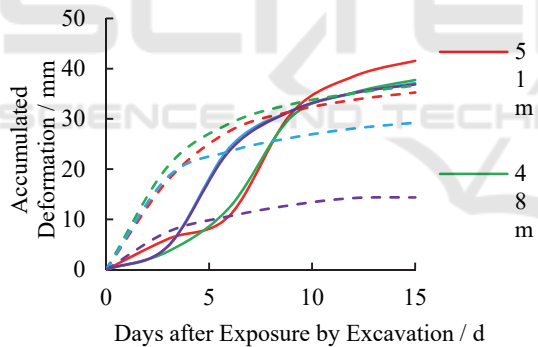

Figure 8: Calculated values for accumulative subsidence after exposure at different locations.

Variation of arch settlement of each measuring point during tunneling into the fractured band is further analyzed, and a three-dimensional surface map is drawn as shown in Figure 7. The accumulated settlement distribution of each measuring section is plotted in as tunnel face is advancing. The negative value in distance between the monitored section and the fractured zone indicates that the monitored section is located behind the fractured zone. The distance between tunnel face and the fractured zone varies from 48m to 0. Result shows that when the tunnel face is constantly advancing to the fractured zone, the settlement of surrounding rockmass is quite different on each monitoring section.

Given the ideal situation in the actual monitoring, in which monitoring starts once the section is exposed by excavation, the settlement variation of the monitored sections in different distance to the fractured zone are plotted as separate curves. Accumulative settlement deformation of each monitoring section is shown in Figure 8. Observation shows the accumulative deformation value of the monitored section 51m away from the fractured zone is the largest, while that 21m away from the fractured zone is the smallest. As shown in Figure 7, the total accumulative deformation of the monitored section closer to the fractured zone is larger (including the deformation before the monitored section is exposed). On the other hand, the complete deformation time curve of the monitored section should have an inflection point. In the deformation accelerating period from the beginning of the deformation, the deformation rate is increasing, while the deformation rate will be decreasing, after the inflection point. If the deformation curve of the monitored section at different distances from the fractured zone is a function of time as Equation 7.

$$\delta(x) = f(x, t) \tag{7}$$

When x is determined, the function should have an inflection point at $t > 0$, and the inflection point would not be monitored when there is a fractured zone at a certain distance in front.
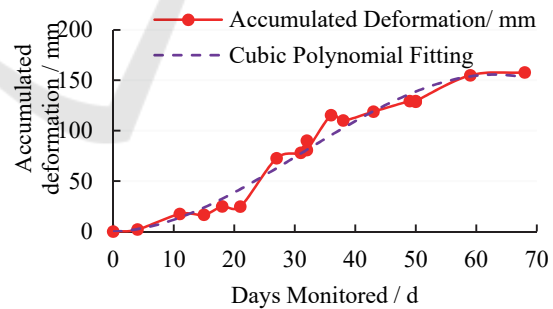

Figure 9: Statistical analysis of accumulative deformation measured at different monitoring sections.

The relationship between monitoring date and accumulative settlement deformation of different sections is shown in Figure 9, from which comprehensive analysis is carried out on the monitored data of the tunnel sections between DK330+029 and DK330+115. Rockmass quality change is very small among there sections, while no fractured zone was found. On February 18, 2013, the

accumulative settlement value of the top arch has a significant inflection point in the fitting curve.

Cubic polynomial is used to fit monitored deformation, for further study on identifying the inflection point on the deformation curve, as Equation 8, with correlation coefficient of 98.6%.

$$Y = -0.0012x^3 + 0.1117x^2 + 0.1866x \qquad (8)$$

Given the second derivative of $Y(x)$ being 0, the inflection point position $X \approx 31$d. It means that on the deformation curve, deformation rate changes from continuously increasing to reducing on the 31st day. However, compared with Figure 6, it is found that the inflection point was not observed in the deformation-time curve monitored after the section around the fractured zone is exposed. It is indicated that the deformation of this section has already been influenced by the excavation area before this section being exposed by excavation. Actual accumulative deformation should be larger. It can also be seen from Figure 7 that the inflection point in the deformation-time curve on the section closer to the fractured zone should occur before the section is exposed by excavation, i.e. $X_i < 0$.

4.3 Influence of Inclined Angle on Deformation Curve of Surrounding Rockmass

The deformation of the surrounding rockmass caused by tunnel excavation through fractured zone in different inclinations are analyzed. As analyzed by similar method as shown in Figure 9, the position of the inflection point on the settlement deformation curves of sections in various axial distances to the fractured zone are shown in Table 4.

As observed, under the influence of specific inclination angle of the fractured zone, the inflection point would appear sooner after the section is exposed, when the section is closer to the fractured zone. The change in inclination angle of the fractured zone has a great influence on when the inflection point would appear. When the inclination angle is small, the inclination change has a greater effect on the change of the inflection point position on time domain. When the inclination angle is close to 90°, the inflection position is not sensitive to inclination angle. However, when the inclination angle is smaller, the location of inflection point on the deformation-time curve is much more sensitive. For example, when the inclination angle is 100°, if the section is monitored right after exposure, the inflection point can still be monitored a few days later. So as to determine a

possible existence of a fractured zone several tens of meters ahead the monitored section. Thus timely adjustment can be applied to excavation and support parameters, to avoid a potential large-scale construction disasters.

Table 4: Inflection point position of different monitoring sections due to inclination change of fractured zone.

Distance to Fractured Zone / m	Inclination angle of fractured zone / °										
	40	50	60	70	80	90	100	110	120	130	140
51	-6	-1	3	6	7	8	10	11	12	13	15
42	-9	-4	0	2	4	6	8	9	10	12	14
33	-13	-8	-4	0	1	3	5	7	8	10	12
21	-18	-12	-7	-3	-1	1	3	5	6	8	11

5 CONCLUSION

Analysis of the collapse disaster during the blasting excavation of the Lanzhou-Xinjiang high-speed railway, due to the existence of a fractured zone. The selection of reasonable blasting parameters is of great significance to avoid the construction disaster caused by fractured zone. Following conclusions can be drawn based on theoretical and numerical analysis on the monitored data of surrounding rockmass deformation in different tunnel section.

(1) The deformation rate of surrounding rockmass in increases first and then decreases along tunnel axis, when rockmass integrity is high and even. And there is an inflection point on the deformation-time curve. By observing the occurrence date of the inflection point after section exposure, the possibility of fractured zone ahead can be estimated, and reasonable adjustment can be applied to excavation and support blasting excavation parameters to avoid construction disasters.

(2) The deformation process of the surrounding rockmass is obviously affected by fractured zone in vicinity, which makes a sooner appearance of the inflection point on deformation-time curve. Under the same circumstance, the surrounding rockmass near the fractured zone may even generate a large portion of deformation before excavation, and the inflection point may disappear in the monitored deformation curve from the exposure of the section. And the deformation rate might only be reducing after the excavation.

(3) When the inclination angle of the fractured zone is small, the location of inflection point on deformation-time curve is more sensitive to the change of inclination angle. And it is much less sensitive to the inclination angle, when it is close to 90°.

ACKNOWLEDGEMENTS

REFERENCES

Alejano, LR., Rodriguez-Dono, A., Veiga, M., 2012. Plastic radii and longitudinal deformation profiles of tunnels excavated in strain-softening rock masses. Tunnelling and Underground Space Technology, 30: 169-182.

Basarir, H., Genis, M., Ozarslan, A., 2010. The analysis of radial displacements occurring near the face of a circular opening in weak rock mass. International Journal of Rock Mechanics and Mining Sciences, 47(5): 771-783.

Cai, Y., Jiang, Y., Djamaluddin, I., Iura, T., Esaki, T., 2015. An analytical model considering interaction behavior of grouted rock bolts for convergence-confinement method in tunneling design. International Journal of Rock Mechanics and Mining Sciences, 76: 112-126.

Carranza-Torres, C., Fairhurst, C., 2000. Application of the convergence-confinement method of tunnel design to rock masses that satisfy the Hoek-Brown failure criterion. Tunnelling and Underground Space Technology, 15(2): 187-213.

China Railway First Surver and Design Institute Group CO., LTD. 2010. Risk Evaluation Report for Daliang Tunnel of Gansu-Qinghai Section on New Second Lanzhou-Urumqi Double-track Railway.

Cui, L., Zheng, J., Zhang, R., Zhang, W., 2014. Study of support pressure and surrounding rock deformation of a circular tunnel with an elastoplastic softening model. Rock and Soil Mechanics, 35(3): 717-722+728.

Fatemi Aghda, S., Ganjalipour, K., Esmaeil Zadeh, M., 2016. Comparison of Squeezing Prediction Methods: A Case Study on Nowsoud Tunnel. Geotechnical and Geological Engineering, 34(5): 1487-1512.

Hoek, E., 1988. In The Hoek-Brown failure criterion-a 1988 update, Proc. 15th Canadian Rock Mech. Symp, 'Ed.' Toronto, Dept. Civil Engineering, University of Toronto, p: 31-38.

Institute of Rock and Soil Mechanics, Chinese Academy of Sciences, 2012. High In-situ Stress and Surrounding Rockmass Deformation Report for Daliang Tunnel of Gansu-Qinghai Section on New Second Lanzhou-Urumqi Double-track Railway.

Kun, M., 2013. Onargan T. Influence of the fault zone in shallow tunneling: A case study of Izmir Metro Tunnel. Tunnelling and Underground Space Technology, 33: 34-45.

Lenz, G., Kluckner, A., Holzer, R., Stadlmann, T., Schachinger, T., Gobiet, Gl., 2017. Prediction of fault zones based on geological and geotechnical observations during tunnel construction. Geomechanics and Tunnelling, 10(4): 366-379.

Lin, D., Yuan, R., Shang, Y., Bao, W., Wang, K., Zhang, Z., Li, K., He, W., 2017. Deformation and failure of a tunnel in the restraining bend of a strike-slip fault zone: an example from Hengshan Mountain, Shanxi Province, China. Bulletin of Engineering Geology and the Environment, 76(1): 263-274.

Lisjak, A., Garitte, B., Grasselli, G., Muller, HR., Vietor, T., 2015. The excavation of a circular tunnel in a bedded argillaceous rock (Opalinus Clay): Short-term rock mass response and FDEM numerical analysis. Tunnelling and Underground Space Technology, 45: 227-248.

Lu, AZ., Chen HY., Qin, Y., Zhang, N., 2014. Shape optimisation of the support section of a tunnel at great depths, Computers and Geotechnics, 61: 190-197.

Moffat, R., Sotomayor, J., Beltran, JF., 2015. Estimating tunnel wall displacements using a simple sensor based on a Brillouin optical time domain reflectometer apparatus. International Journal of Rock Mechanics and Mining Sciences, 75: 233-243.

Panet, M., 1995. Le calcul des tunnels par la méthode convergence-confinement. 'Ed.' Presses ENPC.

Vlachopoulos, N., Diederichs, MS., 2009. Improved Longitudinal Displacement Profiles for Convergence Confinement Analysis of Deep Tunnels. Rock Mechanics and Rock Engineering, 42(2): 131-146.

Zhang, G., Jiao, Y., Wang, H., 2014. Outstanding issues in excavation of deep and long rock tunnels: a case study. Canadian Geotechnical Journal, 51(9): 984-994.

Zhao, K., Bonini, M., Debernardi, D., Janutolo, M., Barla, G., Chen, GX., 2015. Computational modelling of the mechanised excavation of deep tunnels in weak rock. Computers and Geotechnics, 66: 158-171.